Journal of Animal & Plant Sciences (J.Anim.Plant Sci. ISSN 2071-7024)
Vol.68(3) : 13535 -13555 *https://doi.org/10.35759/JAnmPlSci.v68.3.5*

Computational repurposing of potential inhibitors targeting leishmanial DNA topoisomerase IB

Mariam Salem Alghamdi [*1], Saeed M. N. Alasmari [2], Maryam Abdulrahman Alahdal[3], Ahmed Saif [4]

[1,3] Department of Biology, Faculty of Sciences, Umm Al-Qura University, Makkah 24381, Saudi Arabia
[2] Department of Biology, Faculty of Science and Arts, Najran University, 1988 Najran, Saudi Arabia.
[4] Department of Clinical Laboratory Sciences, College of Applied Medical Science, King Khalid University, Abha 61321, Saudi Arabia

* Correspondence: msghamidy@uqu.edu.sa ORCID ID: https://orcid.org/0000-0002-7778-1875
SMNA: smalasmari@nu.edu.sa ORCID ID: https://orcid.org/0009-0006-4407-6172
Ma: Mayahdal@uqu.edu.sa
AS: amsaif8080@gmail.com ORCID ID: https://orcid.org/0000-0002-9614-3238

Keywords: AMG900, Lifitegrast, *Leishmania donovani*, MD simulation, Molecular docking

Submitted 25/05/2026, Published online on 31st July 2026 in the *Journal of Animal and Plant Sciences (J. Anim. Plant Sci.) ISSN 2071 – 7024*

1 ABSTRACT

Leishmanial DNA topoisomerase IB (LdTOP1) is an appealing drug target owing to its crucial roles during DNA replication and transcription. The increasing drug resistance towards anti-leishmanial chemotherapeutics necessitates the search of alternative drugs that overcome the current resistance mechanisms. This study employed the computational approach to repurpose currently approved drugs as well as those in the preclinical stage but well characterized biologically. Molecular dynamics (MD) simulation was performed to investigate LdTOP1 flexibility and to sample possible conformers for subsequent virtual screening of the selected chemical libraries. Top potential hits from the initial virtual screening were subjected to exhaustive molecular docking to find more accurate binding poses and binding affinities. To validate the docking results, unbiased MD simulations and free energy calculation via Molecular Mechanics with Generalized Born Surface Area were employed. Computational simulations and free energy calculations suggest Lifitegrast is a potential LdTOP1 inhibitor. The interactions of Lifitegrast suggest it would bind and affect LdTOP1 in a different way than currently known topoisomerase inhibitors to which mutation-based resistance is already known. The suggested modulators could provide an opportunity to rapidly develop antileishmanial drugs by eliminating the toxicity testing since these two molecules (Lifitegrast and AMG900) are well-characterized in terms of their pharmacokinetic profiles. Validation of these findings and further investigation to determined how the molecules affect the function of LdTOP1 are worth investigations.

2 INTRODUCTION

Vector-borne infections are one of the major threats to human health globally, especially in tropical and subtropical regions (Chala & Hamde, 2021). One of such diseases is Leishmaniasis, an infection with a species of the intracellular protozoan *Leishmania* that harbours more than 20 species, all of which can cause the disease. The infection is mostly asymptomatic but in the symptomatic cases the manifestations are diverse and range from mild cutaneous lesions to a life-threatening sever visceral infection. The disease is transmitted through the bites of an infected female sandflies (Diptera: Psychodidae) hence, it endemic to numerous

regions and affect more than 12 million people worldwide with a fatality rate of 30,000 cases annually (Mathison & Bradley, 2023). The regulation of DNA topology is a pivotal process to sustain efficiency of gene regulation pathways. DNA unwinding during transcription or replication triggers torsional stress and DNA supercoiling that can block the progress of the transcription or replication (Seol & Neuman, 2016). Despite that DNA negative supercoiling mitigates this torsional stress and eventually aids in DNA strands separation, topoisomerases are still needed for alleviating the stress allowing the replication or transcription machinery to proceed smoothly. Based on their sequences, folds, and reaction mechanisms, eukaryotic DNA topoisomerases are classified into two five families within major categories: Topoisomerases I that contains three families (IA, IB, IC), and Topoisomerase II with two families (IIA, and IIB) (Lamba & Roy, 2022). In Leishmania, type IB topoisomerase (a.k.a. LdTOP1) belongs to the family whose members can relax the positive and negative DNA supercoiling. Leishmanial DNA topoisomerase I (56.6 kDa) has attracted considerable interest as a promising drug target, especially after it was found that Camptothecin (CPT), a plant alkaloid initially developed as an anticancer agent, inhibits this enzyme by promoting the formation of a cleavage complex. Subsequent research confirmed that this mechanism occurs in protozoan parasites as well, and that CPT is toxic to three pathogenic unicellular protozoan parasites: *Trypanosoma brucei, Trypanosoma cruzi,* and *L. donovani* (Reguera *et al.,* 2006). Although FDA has approved two anti-leishmanial drugs, Miltefosine and Amphotericin B, they are both associated with high variations in clinical efficacy, severe side effects such as teratogenicity (Miltefosine), and nephrotoxicity (Pradhan *et al.,* 2022; Sundar *et al.,* 2024). The administration of these drugs might require close monitoring or significant resources for costs and logistics. Drug resistance is also an additional challenge that faces anti-leishmanial treatment (Zhang *et al.,* 2025). Consequently, newer drugs are needed to target key biological processes in the protozoal cells. Natural product isolates such as indoles, lignans, terpenoids, spirooxindole, camptothecin, and various synthetic molecules, including fatty acid analogues and metal complexes, have been reported to show leishmanicidal activity towards DNA topoisomerase IB enzyme (Lee *et al.,* 2021a). Hence, this study aimed to identify potential inhibitor for LdTOP1 from the currently approved drugs or those with enough biological data from pre-clinical studies. The development of drug resistance poses significant challenges in leishmaniasis treatment and has led to an increased interest in identifying new antileishmanial drugs. The repurposing of approved drugs offers a relatively rapid approach that is being advocated globally (Souza Silva *et al.,* 2021). In this work, we suggest that Lifitegrast, an approved medication to treat dry eye syndrome (aka keratoconjunctivitis sicca) as potential modulator of LdTOP1. Computational simulations and free energy calculations support these findings and encourage further experimental testing.

3 MATERIALS AND METHODS

3.1 Topoisomerase modelling : The structure of Topoisomerase I of *L. donovani* with a nicked DNA was modelled by AlphaFold3 (AF3) server (Abramson *et al.,* 2024). The primary sequences for both chains were retrieved from UniProt (IDs A0A3Q8IHS4 & Q8WQM6) and the solved structure (PDB ID: 2B9S). This structure was not directly used due to side chains outliers and missing residues. The quality of the two models was evaluated by MolProbity server (Williams *et al.,* 2018).

3.2 Molecular dynamics simulations : The molecular dynamics of LdTOP1 and its DNA substrate were simulated using CHARMM36m forcefield (J. Huang *et al.,* 2017) in GROMACS 2024.2 (Abraham *et al.,* 2015). The complex was solvated in a water box with the TIP3P water model, and the overall charge was neutralized with Na^+ and Cl^- ions at a

physiological concentration (0.154 M). The system was energetically minimized until no atom had a force >500 kJ/mol/nm. Under periodic boundary conditions, the system equilibration in an NVT ensemble was performed for 2 ns followed by NPT equilibration run for a similar period using the leap-frog integrator. System temperature and pressure were modelled via V-rescale and C-rescale, respectively. Hydrogen atom covalent bonds were constrained via the LINCS algorithm, while long-range electrostatics were modelled by Particle Mesh Ewald (PME) summation. Positional restraints were applied during the equilibration runs and left off in the production run where the parameters used in the NPT equilibration were applied for a run of 100 ns. When a ligand was simulated with Topol I, its parameters and topology were generated obtained from SwissParam server (Bugnon *et al.,* 2023). Trajectory data analysis was done mostly via the built-in functionalities of GROMACS or in MDAnalysis (Michaud-Agrawal *et al.,* 2011). The trajectory was clustered based on the active site residues side chains movement over the simulation. Gromos method with a cutoff of 0.2 nm resulted in 3 clusters that were used

3.3 Virtual screening via molecular docking : Three chemical libraries were downloaded from SelleckChem (www.selleckchem.com/); FDA-approved drugs (n= 3,196), candidate drugs that showed safe administration in humans (passed phase I of clinical trials) (n= 4,213), and the library of pre-clinical compounds (n= 3,603). The libraries were compiled and duplicates were removed via OpenBabel (O'Boyle *et al.,* 2011). Molecules with molecular weight > 1000 Da or < 200 Da were excluded. The canonical SMILES (n=2,208) were fed to Meeko (Santos-Martins *et al.,* 2025) to generate the 3D conformers in a pdbqt file format with conserved bond types and orders. A total of 3,746 ligands were generated (tautomers were also generated) and docked via AutoDock Vina 1.2.5 (Eberhardt *et al.,* 2021) to the active site region in a grid box of 30 x 30 x 30 Å with 0.375Å spacing. The model of AF3 was used as the primary receptor for early molecular docking runs. AF3 model as well as the representative models from clusters were prepared using AutoDockTool script. The top 1280 ligands were subjected to exhaustive molecular docking (exhaustiveness=32), and the top 30 ligands were docked into representative models and the model of AF3 to select the most potential binders.

3.4 Principal component analysis and energy landscape: To eliminate overall rotational and translational movements, MD trajectories were structurally aligned to the protein backbone via least-squares fitting. Covariance matrices of atomic fluctuations were then computed, and principal component analysis (PCA) was performed to extract eigenvectors and eigenvalues describing the global motions. The first two principal components (PC1 and PC2) were projected for each trajectory, and the resulting distributions were smoothed using a kernel density estimator (KDE). Free energy landscapes (FELs) were subsequently obtained by converting the probability density into free energy according to

$$\Delta G = -k_B T \ln (PA - PB)$$

where ΔG is the Gibbs energy landscape, k_B is Boltzmann constant, T is the simulation temperature, and (PA − PB) is the two probabilities of protein during the dynamic pathway. Basins in the FEL correspond to metastable conformational states, separated by energy barriers that reflect transition probabilities between states.

3.5 Free energy calculations : The per-residue decomposition analysis as well as the overall binding free energy of LdTOP1 interactions with the ligands were calculated by gmx_MMPBSA tool for the last 50 ns of the trajectory (Valdés-Tresanco *et al.,* 2021). Molecular Mechanics with Generalized Born Surface Area (MM/GBSA) solvation was the employed approach to estimate binding energy terms over the last half of the simulation time. The analysis used the second model of Onufriev-Bashford-Case (Onufriev *et al.,* 2004) (implemented as gb=5) with internal and external dielectric constants of 2 and 80, respectively.

4 RESULTS AND DISCUSSION

Unlike the monomeric human topoisomerase I, Leishmanial Topo IB (LdTOP1) is a heterodimer composed of two distinct subunits, offering structural divergence from host enzymes. This feature has been exploited to find inhibitors that disrupt the heterodimer protein-protein interaction (Lee *et al.,* 2021b) or potential inhibitors that interfere with DNA binding and catalysis (Kour *et al.,* 2024; Kumar Arya *et al.,* 2024; Saha *et al.,* 2016).

4.1 LdTOP1 is stable and flexible: The quality comparison of the modelled LdTOP1-DNA complex and the solved structure is summarized in Table S1. The predicted model corrected many of the outliers and disfavored angles seen in the experimentally solved model (PDB ID: 2B9S). The two dissimilar protein chains comprise the functional heterodimer of LdTOP1 (Figure 1A). The large chain (LdTOP1L) has three domains; N-terminal domain of 4 α-helices and 2 antiparallel short β-sheets, a middle domain composed of mostly β-sheets with a single helix, and the C-terminal domain that contacts the other chain of the dimer. A long, disordered stretch at the C-terminal end contains 3 non-conserved helices (not solved or modelled). The N-terminus and middle region (M1–R180) of the small chain (LdTOP1S) in the dimer are almost disordered, however, a single helix (S181–A212) is equivalent to a helix (S686–Q713) in the eukaryotic linker domain (Q633–Q713). In many solved structures, region lacks electron density suggesting its high flexibility (Davies *et al.,* 2006; Takahashi *et al.,* 2022), yet unknown function(s). It seems to make contacts with the DNA during removing the torsional coiling, but it is not required for *in vitro* catalysis (Davies *et al.,* 2006). As a typical topoisomerase, LdTOP1 has a toroidal fold that entraps the DNA in a central channel. Domain packing is almost unchanged and no local unfolding was observed upon secondary structure analysis of the apo and the holo systems (Figure S1), and stable volume and density of the systems over simulation (Figure S2A). This is consistent with the experimental findings of archaeal TOP1 apo structure recently solved in its native conformation (Takahashi *et al.,* 2022). The middle channel of LdTOP1 carry high positive charge to accommodate the negatively charged DNA sugar-phosphate backbone. The DNA passes through the central channel of LdTOP1 and makes contacts with both chains of the dimer (Figure 2A). The N-terminal domain of the large chain is not involved in direct contact with the DNA, but it seems to provide structural support to the loops of the middle domain that wraps around the DNA (Figure 2B).

Journal of Animal & Plant Sciences (J.Anim.Plant Sci. ISSN 2071-7024)
Vol.68(3) : 13516 -13524 https://doi.org/10.35759/JAnmPlSci.v68.3.5

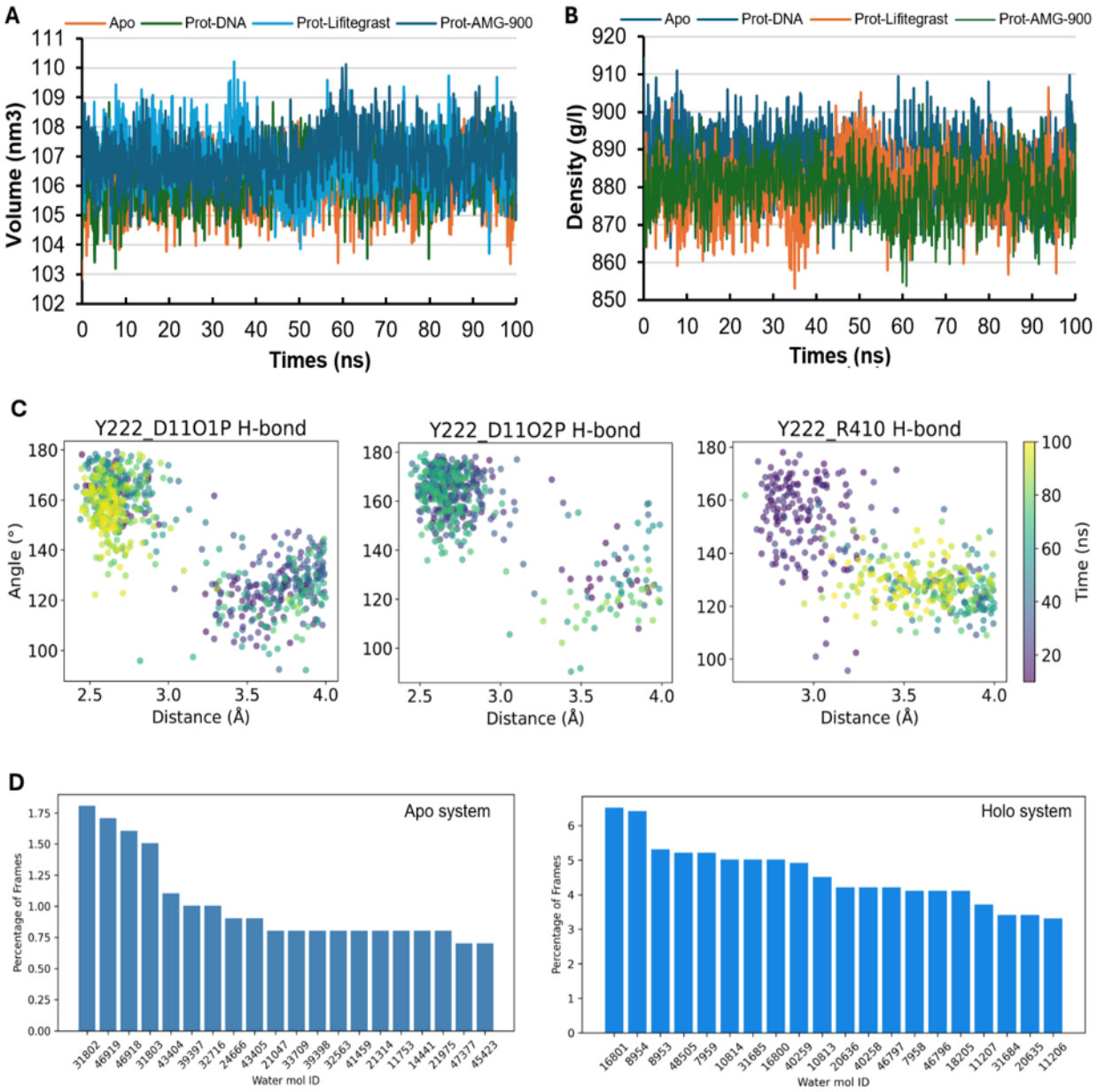

Figure S2. A and B) Volume and density of the systems over the simulation. **C)** Hydrogen bonds with Y222 in the nicked DNA system. The distance refers to the hydrogen-acceptor distance in Angstroms. **D)** Water residency time around over the simulation of the LdTOP1-DNA complex.

Table S1. Quality evaluation of the solved and modelled structures of LdTOP1-DNA complex.

All-Atom	Criterion	Solved (PDB ID:2B9S)		AF3 model		Goal
		n	%	n	%	
	Clashscore, all atoms:	2.69 (N=356)		4.5 (N=1784)		
Protein Geometry	Poor rotamers	11	0.0301	9	0.0211	<0.3%
	Favored rotamers	329	0.8989	410	0.9602	>98%
	Ramachandran outliers	0	0	0	0	<0.05%
	Ramachandran favored	455	0.964	427	0.9854	>98%
	Rama distribution Z-score	-1.71 ± 0.33		1.82 ± 0.36		abs(Z score) < 2
	MolProbity score	1.66		1.47		
	Cβ deviations >0.25Å	5	0.0109	0	0	0
	Bad bonds	2 / 3817	0.0005	0 / 4092	0	0%
	Bad angles	2 / 5195	0.0004	0 / 5525	0	<0.1%
Peptide Omegas	Cis Prolines	0 / 24	0	0 / 25	0	≤5%
	Twisted Peptides	1 / 475	0.0021	-	-	0
Nucleic Acid Geometry	Bad bonds	0 / 996	0	4 / 1012	0.004	0%
	Bad angles	27 / 1530	0.0176	6 / 1559	0.0038	<0.1%
Low-resolution Criteria	CαBLAM outliers	-	-	4	0.008	<1.0%
	CA Geometry outliers	-	-	1	0.0021	<0.5%

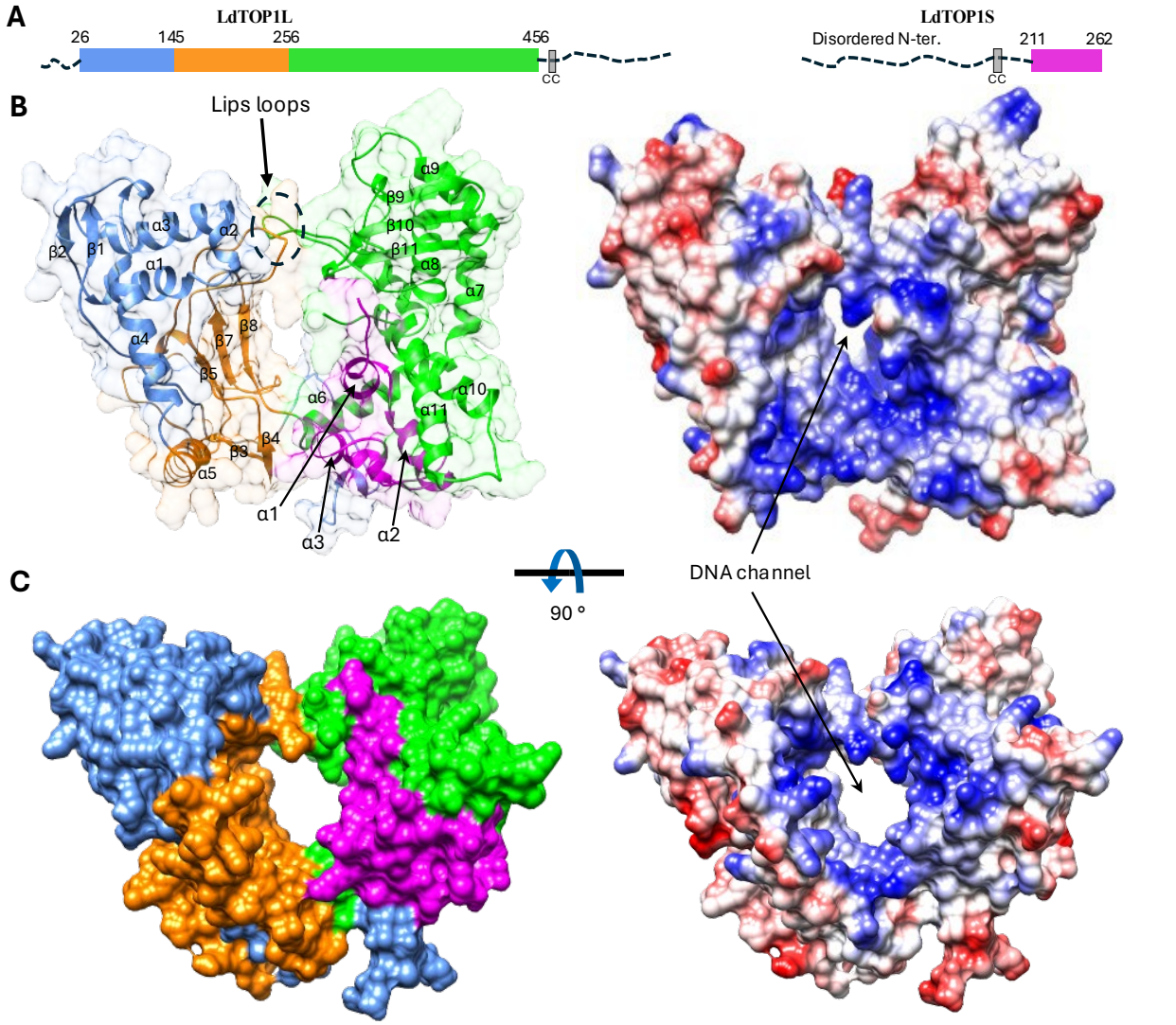

Figure 1. Domain arrangement and structure of LdTOP1. A) domain boundaries for both chains are color-coded to match the cartoon and surface representations. B) cartoon and surface representation of LdTOP1 where LdTOP1L is

shown in cyan, while LdTOP1S is in magenta. C) The electrostatic surface of the upper panel to show the positively charged channel for the DNA.

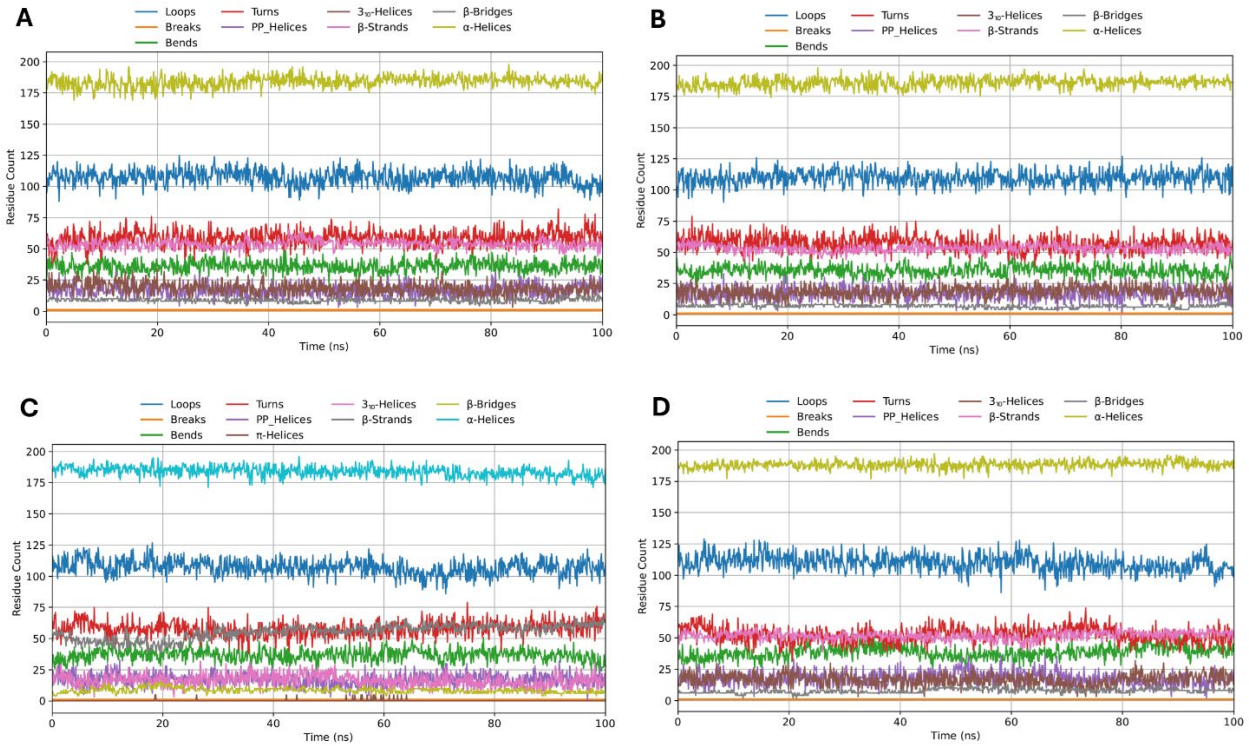

Figure S1. Secondary structures in the systems over the simulation period.

The superimposition of LdTOP1 with the human counterpart (PDB ID: 1EJ9) is also shown in Figure 2C (RMSD 1.64 Å). To mimic the active state, LdTOP1 was modelled with a double stranded DNA but the strand facing the conserved residues was nicked as in the vanadate solved structure (PDB ID: 2B9S). The active site residues (Lys352, Asp353, Arg310, Arg413, and His453 on LdTOP1L and Thr217, Asn221, and Tyr222 on LdTOP1S) coordinate DNA positioning for the catalysis via the conserved pentad residues (Lys352, Arg310, Arg413, His453, and Tyr222) (Figure2 D). It has been shown that alanine mutagenesis of Arg-314, Lys-352, Arg-410, and His-453 in LdTOP1L abolished the topoisomerase activity (Diaz-González *et al.,* 2008). Furthermore, substitution of Tyr-222 in LdTOP1S with phenylalanine abolished the activity as well.

Proteins are dynamic biomolecules, and their conformational ensemble can be explored via MD simulations (Filipe & Loura, 2022). To investigate the structural dynamics of the apo form of LdTOP1 and obtain a reasonable conformation for downstream virtual screening, the DNA strands were removed, and the dimer underwent unbiased all-atom MD simulation for 100 ns. Over the simulation, the apo form experienced large-scale movement in comparison to the holo form (Figure 3A) (average RMSD ± SD: 5.43 ± 1.95 Å vs 1.94 ± 0.29 Å). The RMSD of 95% of the frames of the holo structure would fall between 2.53 and 1.35 Å of the predicted model, whereas the apo form frames would be between 9.32 and 1.54 Å.

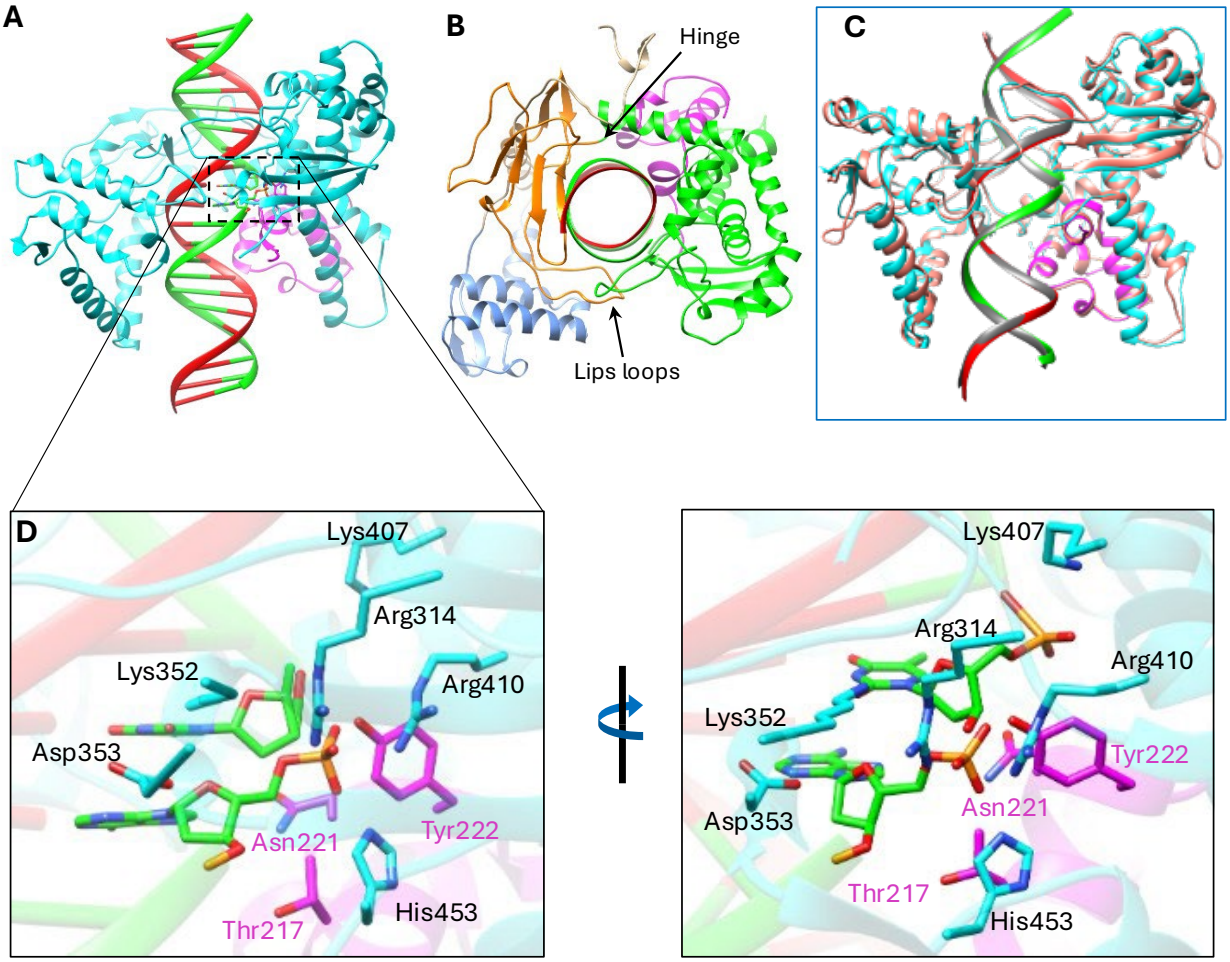

Figure 2. Holo structure of LdTOP1 with DNA substrate. A and B are different views for LdTOP1 while C is a superimposition of LdTOP1 with the human counterpart topoisomerase (PDB ID: 1K4T). D) The catalytic residues' arrangement at the active site with nicked DNA.

Such conformational changes are expected as the domains of such proteins are only stabilized when the natural substrate (DNA) is bound. This large-scale movement has been captured experimentally in the topoisomerase of the hyperthermophilic archaeon *Caldiarchaeum subterraneum* (Takahashi *et al.,* 2022). The residues that experienced the most fluctuations are in the large subunit only in the absence of DNA where the conformational changes are prominent and side chains are freely interacting with the solvent. The flexibility of LdTOP1 is mediated by a short hinge loop (M254-S258) between the N-terminal and the middle domains (Figure 3B). The LdTOP1S retains its interaction and binding conformation with the C-terminal domain. Tyr222 is a key residue for catalysis by a nucleophilic attack on the sugar-phosphate backbone of the DNA and inducing the break of a phosphodiester bond. Over the simulation time, Tyr222 established stable hydrogen bond with the free phosphate moiety of the nicked DNA (Figure S2B) with an average distance between the hydrogen and the acceptor atom of 3.02 ± 0.41 Å and angle of 149.22 ± 17.30°. Water molecules around Tyr222 are believed to activate Tyr222 nucleophile attack by acting as a base that accepts a proton from the Tyr222 OH during catalysis. The MD simulation has detected few water molecules that spent more time near the OH of Tyr22 in the holo system than in the apo form (Figure S2C). This might support the previous inconclusive results of water contributions to catalysis in studies on

human topoisomerase (Redinbo *et al.,* 2000). Topoisomerase I cuts and reseals DNA by a transesterification in which the enzyme's active-site tyrosine attacks the DNA backbone and the liberated 5'-OH of the DNA (not water) re-attacks to re-ligate. However, water can hydrolyze the enzyme–DNA (3'-phosphotyrosyl) intermediate under certain conditions (or when re-ligation is blocked), producing an irreversible break that is subsequently repaired (Krogh & Shuman, 2000).

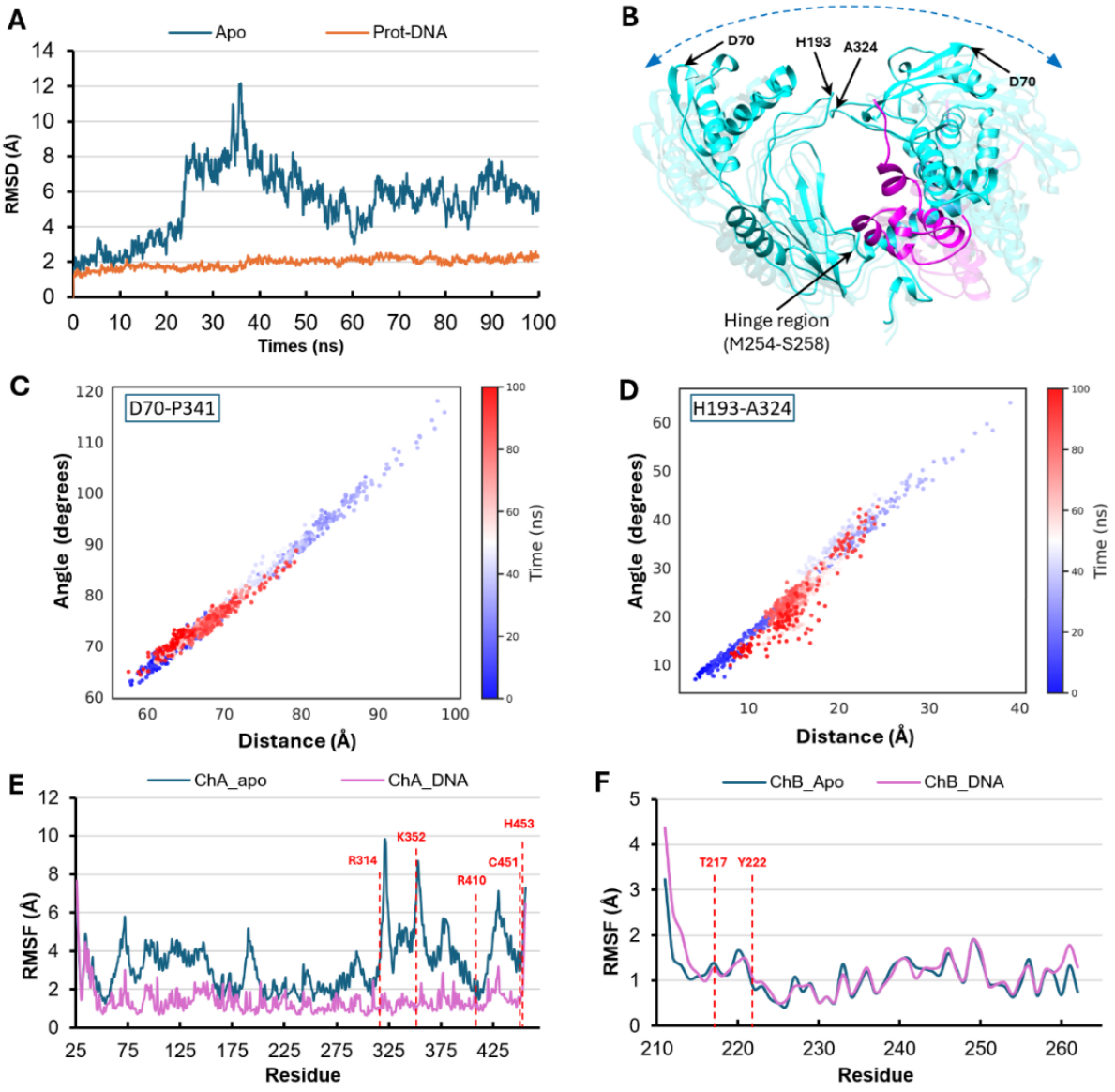

Figure 3. Structural dynamics of the apo vs the holo (with DNA) forms of LdTOP1. A) RMSD of protein backbone and DNA. B) the conformational space sampled by the apo form over the course of simulation (100 ns). C and D) Angle and distance analysis of LdTOP1 opening in the apo state. E and F) RMSF of LdTOP1 residues in the apo and the holo states. Catalytic residues are marked with dashed lines and labels.

It's well-known that this tyrosine is conserved, and it forms a transient covalent bond with the nicked DNA during the removal of topological torsions (Soren *et al.,* 2020). Most of topoisomerases IB inhibitors exert their inhibitory effect by stabilizing the enzyme-DNA

covalent state and some of them (camptothecin, Hydrotopotecan) intercalate between the bases of the DNA (Chrencik *et al.,* 2004; Staker *et al.,* 2002).

4.2 Lifitegrast is a potential inhibitor with unique interactions: From the screened molecules, 175 showed binding affinity < −8.00 kcal/mol. The molecules with predicted binding affinity < −9.0 kcal/mol were subjected to exhaustive docking and the best 4 molecules were visually inspected to select the ones with favorable interactions with LdTOP1. Among the top potential modulators/inhibitors, Lifitegrast, AMG900, RAF265, and Nilotinib scored the top binding affinities (Figure 4A). Lifitegrast is an approved drug for dry eye syndrome while the remaining three molecules are kinase inhibitors. All the four hits were predicted to establish contacts with at least four charged residues at the central DNA channel, namely, Arg314, Arg410, N317, and Lys352 (Figure 4B-E). AMG900 were predicted to establish eight hydrogen bonds with LdTOP1, mostly with Arg314 and Arg410 (5 bonds) and S331 and E318 with an average length of 3.27 ± 0.40 Å (mean ± SD). Similarly, six hydrogen bonds were predicted between Lifitegrast and LdTOP1 key residues: G316 (backbone N) Arg314, N317 (backbone N and side chain), and Tyr222 (overall length 3.07 ± 0.18 Å). Nilotinib has 2 hydrogen bonds with Arg314 (3.27 Å) and Lys319 (3.22 Å) while RAF265 established a single hydrogen bond with R314 (3.27 Å). Herein, AMG900 and Lifitegrast established unique interactions with LdTOP1 residues that are different from the ones involved in conferring camptothecin resistance. Based on visual evaluation of of atomic interactions, Lifitegrast and AMG900 were selected for downstream analysis. Camptothecin was originally developed as an anticancer drug but showed anti-leishmanial activity by inhibiting LdTOP1 (Bodley *et al.,* 1995). Previous studies have shown that camptothecin resistance in Leishmania is mediated by target protection mutations in LdTOP1L as well as by efflux pump (BoseDasgupta *et al.,* 2008; Diaz-González *et al.,* 2008; Marquis *et al.,* 2005). Specifically, mutations in G195 and D325 or D353 and N221 conferred high levels of resistance to camptothecin (up to 50 µM).

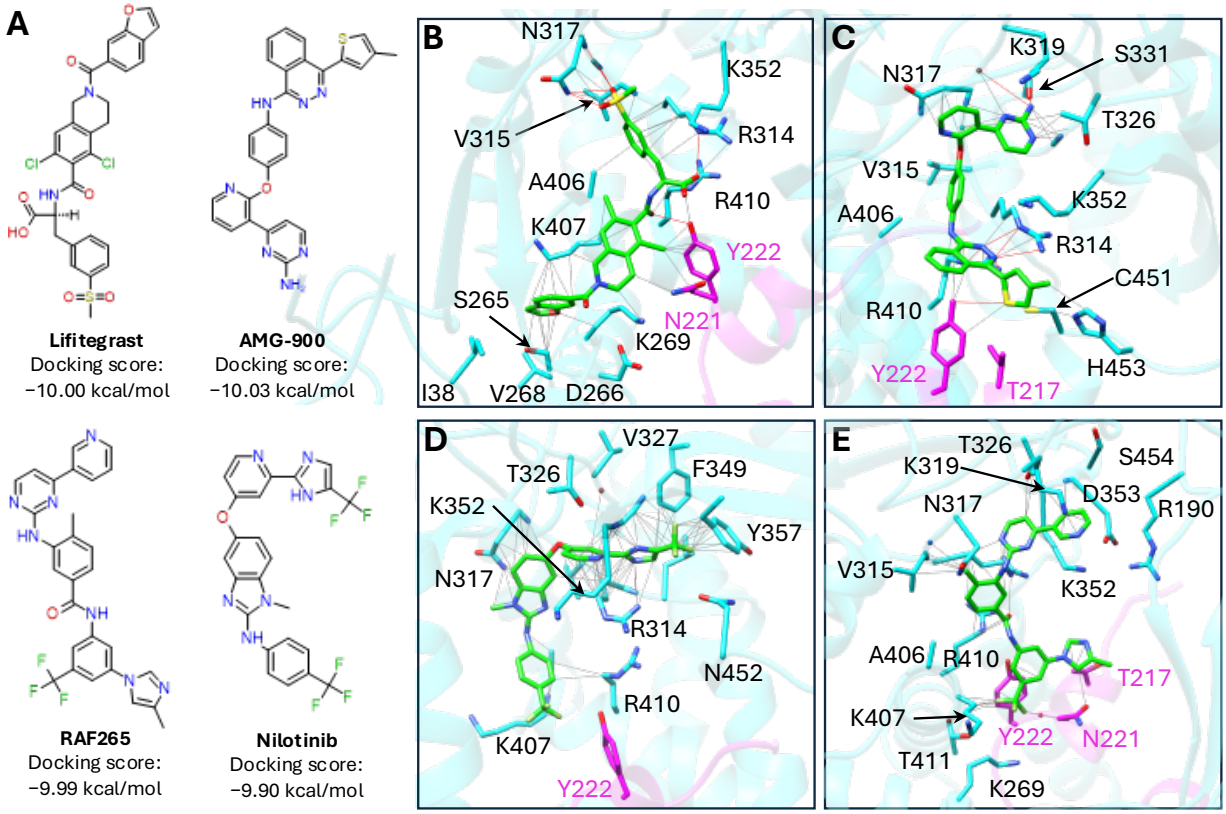

Figure 4. The top 4 promising hits from molecular docking. A) Chemical structures of the molecules along with their docking scores. B) Atomic interactions established by Lifitegrast, C) AMG900, D) RAF265, and E) Nilotinib.

Lifitegrast is an FDA-approved therapeutic agent indicated for the management of keratoconjunctivitis sicca; however, its potential to inhibit topoisomerases has not been investigated. In contrast, AMG900, an Aurora kinase inhibitor, has been experimentally demonstrated to inhibit human DNA topoisomerase IIB (Klaeger *et al.,* 2017). RAF265, another kinase inhibitor with documented anticancer properties through Raf kinase inhibition (T. Huang *et al.,* 2013), was found to lack inhibitory activity against human DNA topoisomerase IIB (Klaeger *et al.,* 2017).Similarly, Nilotinib, a tyrosine kinase inhibitor with reported antiviral efficacy against coronaviruses (García-Cárceles *et al.,* 2022), exhibited no inhibitory effect on either human DNA topoisomerase I or II (Klaeger *et al.,* 2017).

4.3 Lifitegrast is stable over simulation: Establishing a stable protein-ligand complex requires the ligand to undergo a series of conformational changes to sample the most stable conformer with stable interactions with the receptor. The latter also experiences local changes of the residues at the binding site to fits the ligand (Du *et al.,* 2016). In the LdTOP1 context, both Lifitegrast and AMG900 experienced fluctuations over the simulation as seen in their RMSD (Figure 5A). It is worth noting that these fluctuations cannot be attributed to ligand instability only as the receptor pocket is also experiencing motions as seen in the apo system previously. It is not expected from a small molecule ligand to stabilize LdTOP1 as the DNA molecule does. Lifitegrast was more stable than AMG900 after the 50 ns of simulation and most of its fluctuations in the RMDS values are caused by its benzofuran moiety that extends almost freely to the central channel of LdTOP1.

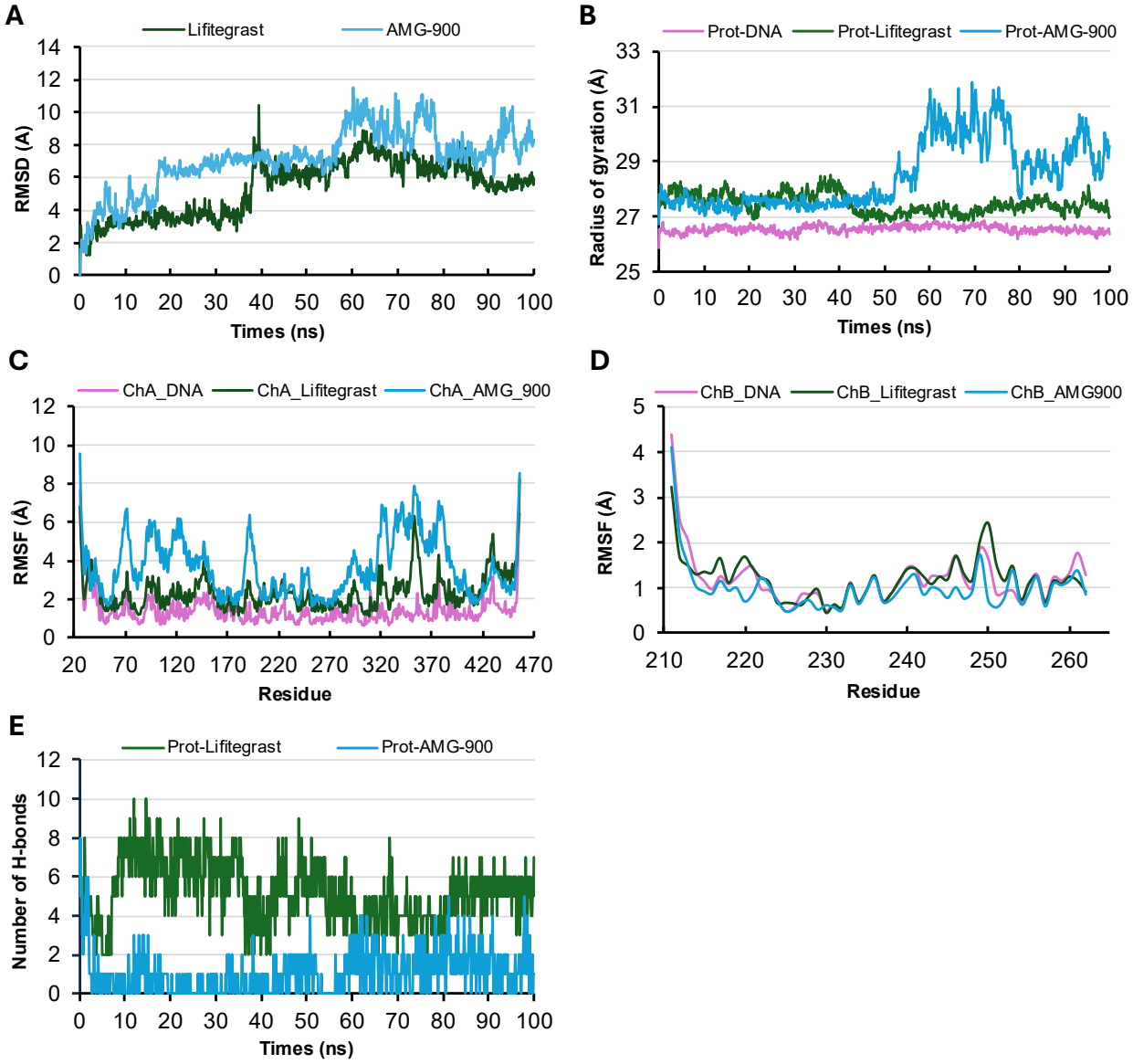

Figure 5. MD simulation of Lifitegrast and AMG900. A) RMSD over the time after firring the complex to the backbone atoms. B) Radius of gyration over the simulation time. C and D) RMSF with special mapping of the catalytic residues. Residues fluctuations when LdTOP1-DNA complex was simulated are included for comparison. E) the number of hydrogen bonds established with the LdTOP1.

Lifitegrast binding, however, restricted the movement of LdTOP1 more than AMG900 as seen in the stable radius of gyration (R_g) over the simulation (Figure 5B). R_g is the root mean square distance of a molecule's atoms from its center of mass, hence it quantifies the spatial distribution of atoms, offering insight into the molecule's compactness or expansion during simulations (Lobanov *et al.,* 2008). It should be noted that the increase of radius of gyration in LdTOP1-AMG900 complex was not due to unfolding events or loss of secondary structures as evidenced by the stable secondary structure analysis (Figure S1). The fluctuations of LdTOP1 residues in the presence of Lifitegrast are almost identical to the fluctuations seen in the holo system (Figure 5C & D), indicating that Lifitegrast, but not AMG900, has the potential to limit local flexibility of LdTOP1 around the catalytic site similar to its state when the natural substrate (i.e. DNA) is bound. This also highlights the structural regions in LdTOP1 whose dynamics are influenced by ligand binding. The majority of interacting residues with Lifitegrast or AMG900 are on LdTOP1L. Only transient interactions were

established with the LdTOP1S. In terms of electrostatic interactions (cationic and hydrogen bonds), Lifitegrast was almost always found interacting with Arg314, Val315, Gly316, Asn317, and Arg410, either with their side chains or the backbone N atoms. Lifitegrast established an average of six stable hydrogen bonds with LdTOP1 that has an average length of 3.08 Å (SD ±0.16) and an average angle of 143.6° (SD ±7.04) (Figure S3). However, AMG900 only sustained 3 hydrogen bonds (Figure 6). Arg314 also established transient π-cation interactions with the methyl phenyl sulfone moiety of Lifitegrast.

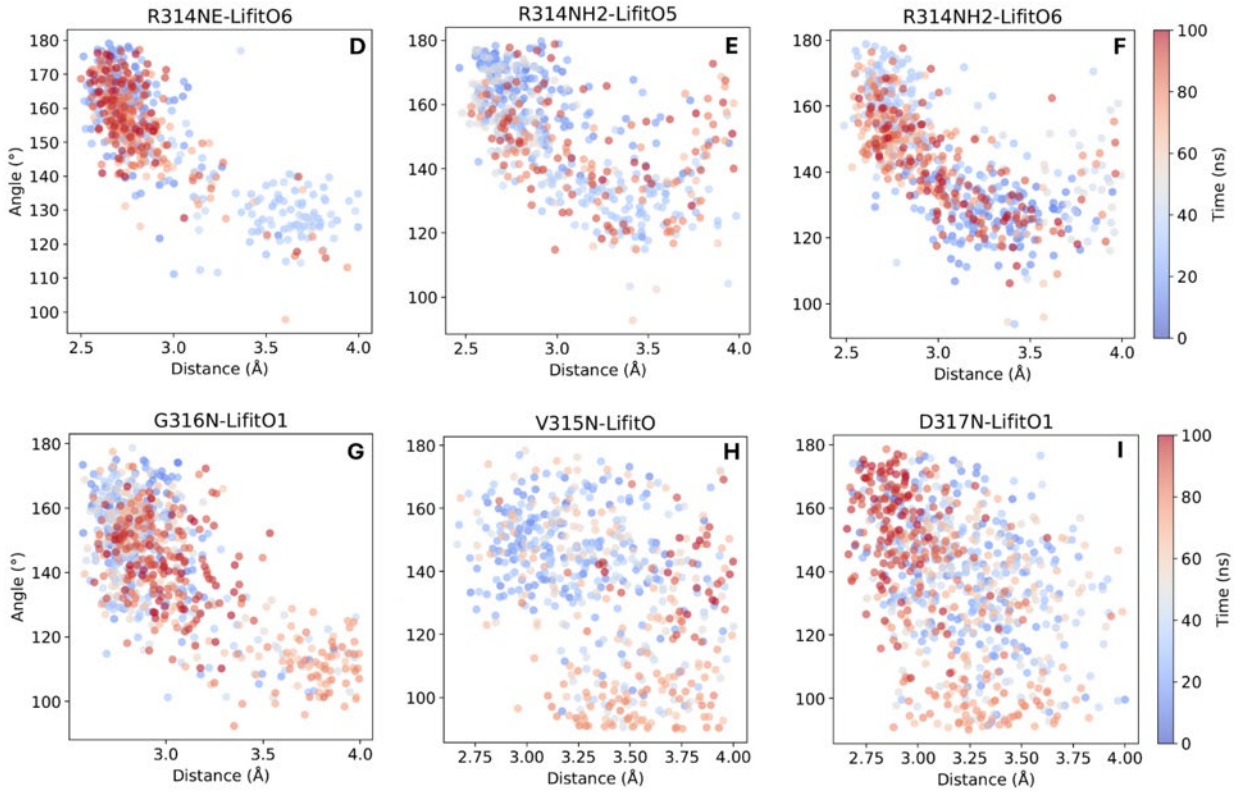

Figure S3.: Lifitegrast-LdTOP1 hydrogen bonds lengths and angles. The most stable bonds are included here to show their length and angles.

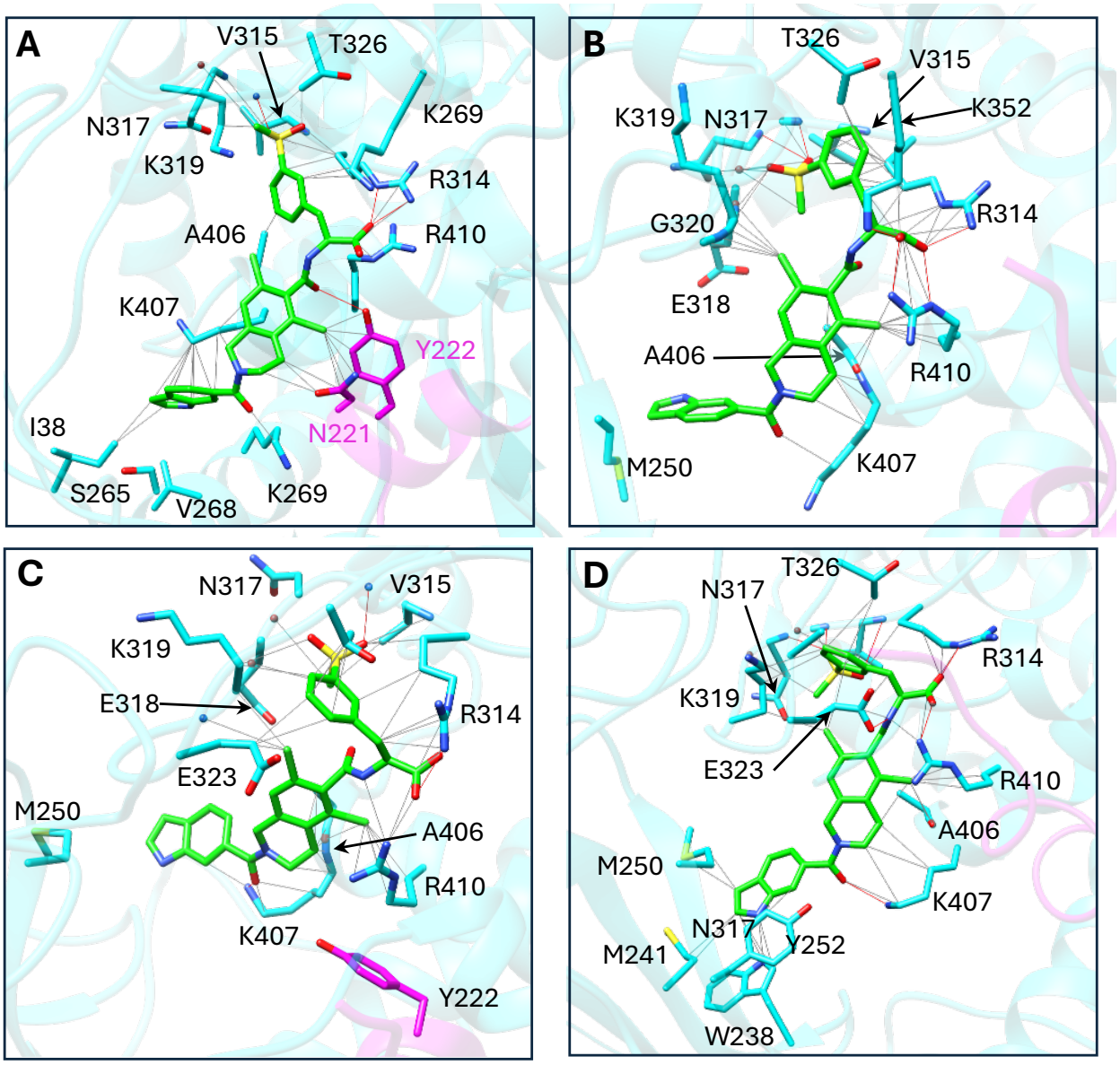

Figure 6. Atomic interaction of LdTOP1-Lifitegrast over the simulation time. A) pose and interaction at 25 ns, B) at 50 ns, C) at 75 ns, and D) at 100 ns. Hydrogen bonds are shown as red lines.

Essential dynamics revealed distinct differences in the conformational motions of LdTOP1 across the apo, DNA-bound, and ligand-bound states. PCA showed that Lifitegrast binding (Figure 7C) reduced the conformational flexibility observed in the apo form (Figure 7A), approaching the restricted dynamics of the DNA-bound state (Figure 7B). The FELs constructed along PC1 and PC2 highlighted the distribution of stable conformational states, with well-defined energy basins representing metastable conformations. These results suggest that ligand binding stabilizes the protein in specific low-energy states, reducing its conformational heterogeneity.

4.4 Free energy estimation favored Lifitegrast :MM/GBSA is widely employed as a post-docking refinement approach in the virtual screening of potential inhibitors due to its balance of computational efficiency and improved accuracy over raw docking scores. By combining molecular mechanics energy terms with implicit solvation models, MM/GBSA provides more realistic estimates of binding free

energies and allows for decomposition into van der Waals, electrostatic, and solvation contributions, thereby elucidating the primary energetic drivers of ligand binding. While MM/GBSA is computationally tractable, allowing for the screening of large ligand sets while reducing the number of candidates subjected to costly synthesis and experimental testing, it has limitations such as the omission of rigorous entropic contributions, dependence on docked pose accuracy, and the approximations inherent to implicit solvent models. The MM/GBSA of Lifitegrast and AMG900 were calculated on the final 50 ns of their simulation trajectories, and the results are summarized in Table 1. Given that the binding pocket is highly positively charged, the MM/GBSA results suggest that inhibitor Lifitegrast exceptionally strong electrostatic interactions (ΔE_{EL} = –251.23 kcal/mol) arise from favorable attraction between its negatively charged or polar groups and the cationic residues in the pocket. However, this advantage is largely offset by the substantial polar solvation penalty (ΔE_{GB} = +258.97 kcal/mol), indicating that desolvation of these polar groups upon binding is energetically costly. In contrast, AMG-900 exhibits much weaker electrostatic interactions (ΔE_{EL} = –22.17 kcal/mol), which is consistent with a less negatively charged or more hydrophobic chemical profile, but benefits from a markedly smaller desolvation penalty (ΔE_{GB} = +46.03 kcal/mol). This trade-off between electrostatic attraction and solvation cost is a well-documented determinant in ligand optimization for charged protein targets (Genheden & Ryde, 2015). The per-residue energy decomposition analysis (Figure S4) shows that Arg314 and Arg410 contribute significantly to the overall binding energy of Lifitegrast in comparison to AMG900.

Journal of Animal & Plant Sciences (J.Anim.Plant Sci. ISSN 2071-7024)
Vol.68(3) : 13516 -13524 https://doi.org/10.35759/JAnmPlSci.v68.3.5

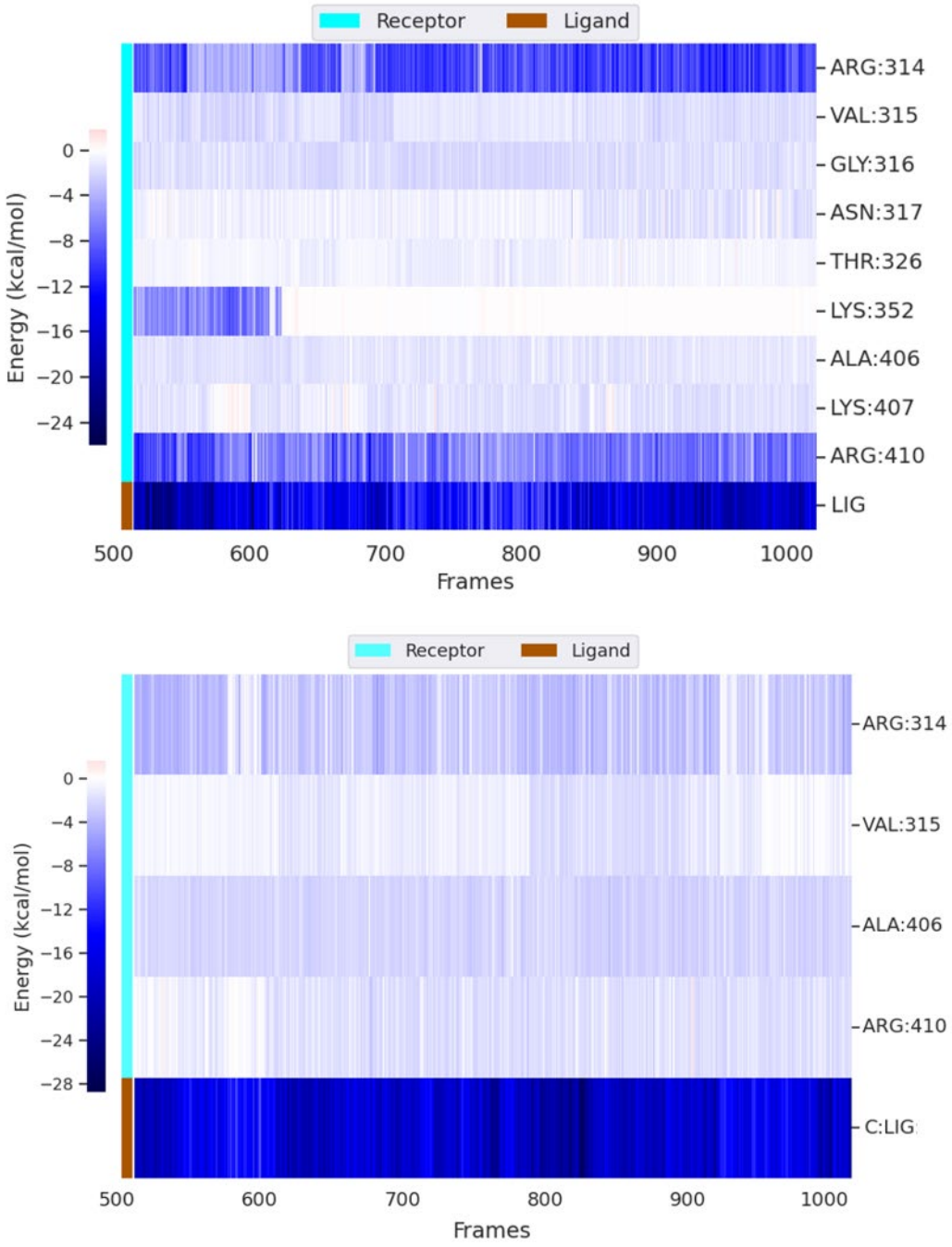

Figure S4: Energy decomposition of the residues involved in Lifitegrast (upper) and AMG900 (lower) binding to LdTOP1 over the simulation time.

Table 1. Free energy estimations of Lifitegrast and AMG900 expressed as average ± SD

Energy component	Lifitegrast	AMG900
$\Delta E_{VDWAALS}$	-42.56 ± 4.99	-51.36 ± 5.06
ΔE_{EL}	-251.23 ± 29.29	-22.17 ± 11.66
ΔE_{GB}	258.97 ± 25.64	46.03 ± 10.25
ΔE_{SURF}	-6.85 ± 0.43	-6.33 ± 0.55
ΔG_{GAS}	-293.8 ± 28.22	-73.53 ± 13.69
ΔG_{SOLV}	252.12 ± 25.53	39.7 ± 9.99
Δ_{TOTAL}	-41.67 ± 7.24	-33.83 ± 5.78

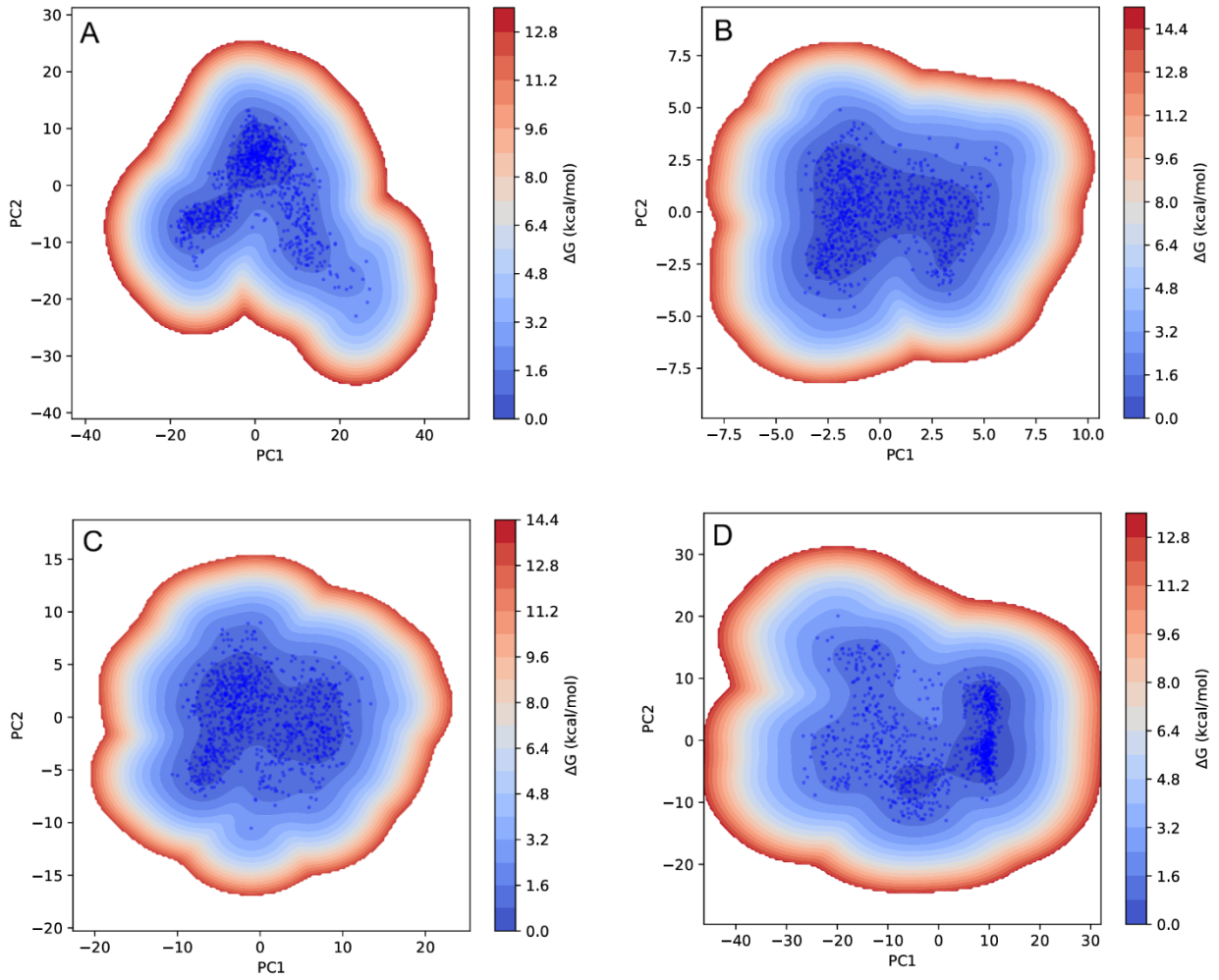

Figure 7: Free energy landscape of LdTOP1 based on principal component analysis of the MD simulation trajectory. (A) LdTOP1 in its apo form, (B) LdTOP1-DNA complex, (C) LdTOP1-Lifitegrast, and (D) LdTOP1-AMG900 complex.

5 CONCLUSION

Drug repurposing remains a cost-effective and efficient strategy for identifying new therapeutic indications, This strategy leverages existing safety data and established mechanisms of action to accelerate the drug development and success rate. procesThis computational repurposing study evaluated potential modulators of LdTOP1 by screening chemical libraries against different conformers generated via MD simulation of the apo form of LdTOP1. In the absence of its natural substrate (DNA), LdTOP1 exhibited notable flexibility; however, binding of Lifitegrast to the DNA central channel restricted this flexibility. Free energy calculations supported these findings. Such conformational changes may impair the physiological function of LdTOP1 by significantly affecting DNA binding. Additionally, other kinase inhibitors were identified as potential binders to the DNA channel, suggesting they may also have disruptive effects. The kinase inhibitors Lifitegrast and AMG900 are promising candidates for inhibiting LdTOP1 via blocking its DNA binding channel.

6 DECLARATION OF INTERESTS

The authors declare that they have no known competing financial interests or personal relationships that could have appeared to influence the work reported in this paper.

Data Availability : The original data generated in the study and the list of repurposed molecules are publicly available on Zenodo via this URL https://zenodo.org/records/17045282

Conflict of interest : The authors confirm the absence of any potential conflict of interest regarding this work or publication. No AI agent was used in this work for generating text or any other purposes.

6 REFERENCES

Abraham, M. J., Murtola, T., Schulz, R., Páll, S., Smith, J. C., Hess, B., & Lindah, E. (2015). GROMACS: High performance molecular simulations through multi-level parallelism from laptops to supercomputers. *SoftwareX*, *1–2*, 19–25. https://doi.org/10.1016/j.softx.2015.06.001

Abramson, J., Adler, J., Dunger, J., Evans, R., Green, T., Pritzel, A., Ronneberger, O., Willmore, L., Ballard, A. J., Bambrick, J., Bodenstein, S. W., Evans, D. A., Hung, C. C., O'Neill, M., Reiman, D., Tunyasuvunakool, K., Wu, Z., Žemgulytė, A., Arvaniti, E., … Jumper, J. M. (2024). Accurate structure prediction of biomolecular interactions with AlphaFold 3. *Nature*, *630*(8016), 493–500. https://doi.org/10.1038/S41586-024-07487-W

Bodley, A. L., Shapiro, T. A., Talalay, P., & Hopkins, J. (1995). Molecular and cytotoxic effects of camptothecin, a topoisomerase I inhibitor, on trypanosomes and Leishmania. *Proceedings of the National Academy of Sciences*, *92*(9), 3726–3730. https://doi.org/10.1073/PNAS.92.9.3726

BoseDasgupta, S., Ganguly, A., Roy, A., Mukherjee, T., & Majumder, H. K. (2008). A novel ATP-binding cassette transporter, ABCG6 is involved in chemoresistance of Leishmania. *Molecular and Biochemical Parasitology*, *158*(2), 176–188. https://doi.org/10.1016/J.MOLBIOPARA.2007.12.007

Bugnon, M., Goullieux, M., Röhrig, U. F., Perez, M. A. S., Daina, A., Michielin, O., & Zoete, V. (2023). SwissParam 2023: A Modern Web-Based Tool for Efficient Small Molecule Parametrization. *Journal of Chemical Information and Modeling*, *63*(21), 6469–6475. https://doi.org/10.1021/ACS.JCIM.3C01053

Chala, B., & Hamde, F. (2021). Emerging and Re-emerging Vector-Borne Infectious Diseases and the Challenges for Control: A Review. *Frontiers in Public Health*, *9*, 715759. https://doi.org/10.3389/FPUBH.2021.715759

Chrencik, J. E., Staker, B. L., Burgin, A. B., Pourquier, P., Pommier, Y., Stewart, L., & Redinbo, M. R. (2004). Mechanisms of Camptothecin Resistance by Human Topoisomerase I Mutations. *Journal of Molecular Biology*, *339*(4), 773–784. https://doi.org/10.1016/J.JMB.2004.03.077

Davies, D. R., Mushtaq, A., Interthal, H., Champoux, J. J., & Hol, W. G. J. (2006). The Structure of the Transition State of the Heterodimeric Topoisomerase I of Leishmania donovani as a Vanadate Complex with Nicked DNA. *Journal of Molecular Biology*, *357*(4), 1202–1210. https://doi.org/10.1016/J.JMB.2006.01.022

Diaz-González, R., Pérez-Pertejo, Y., Pommier, Y., Balaña-Fouce, R., & Reguera, R. M. (2008). Mutational study of the "catalytic tetrad" of DNA topoisomerase IB from the hemoflagellate Leishmania donovani: Role of Asp-353 and Asn-221 in camptothecin resistance. *Biochemical Pharmacology*, *76*(5), 608–619. https://doi.org/10.1016/J.BCP.2008.06.019

Du, X., Li, Y., Xia, Y. L., Ai, S. M., Liang, J., Sang, P., Ji, X. L., & Liu, S. Q. (2016). Insights into Protein–Ligand Interactions: Mechanisms, Models, and Methods. *International Journal of Molecular Sciences*, *17*(2), 144. https://doi.org/10.3390/IJMS17020144

Eberhardt, J., Santos-Martins, D., Tillack, A. F., & Forli, S. (2021). AutoDock Vina 1.2.0: New Docking Methods, Expanded Force Field, and Python Bindings. *Journal of Chemical Information and Modeling*, *61*(8), 3891–3898. https://doi.org/10.1021/ACS.JCIM.1C00203

Filipe, H. A. L., & Loura, L. M. S. (2022). Molecular Dynamics Simulations: Advances and Applications. *Molecules*, *27*(7), 2105. https://doi.org/10.3390/MOLECULES27072105

García-Cárceles, J., Caballero, E., Gil, C., & Martínez, A. (2022). Kinase Inhibitors as Underexplored Antiviral Agents. *Journal of Medicinal Chemistry*, *65*(2), 935–954. https://doi.org/10.1021/ACS.JMEDCHEM.1C00302

Genheden, S., & Ryde, U. (2015). The MM/PBSA and MM/GBSA methods to estimate ligand-binding affinities. *Expert Opinion on Drug Discovery*, *10*(5), 449–461. https://doi.org/10.1517/17460441.2015.1032936

Huang, J., Rauscher, S., Nawrocki, G., Ran, T., Feig, M., de Groot, B. L., Grubmüller, H., & MacKerell, A. D. (2017). CHARMM36m: an improved force field for folded and intrinsically disordered proteins. *Nature Methods*, *14*(1), 71–73. https://doi.org/10.1038/nmeth.4067

Huang, T., Karsy, M., Zhuge, J., Zhong, M., & Liu, D. (2013). B-Raf and the inhibitors: From bench to bedside. *Journal of Hematology and Oncology*, *6*(1). https://doi.org/10.1186/1756-8722-6-30

Klaeger, S., Heinzlmeir, S., Wilhelm, M., Polzer, H., Vick, B., Koenig, P. A., Reinecke, M., Ruprecht, B., Petzoldt, S., Meng, C., Zecha, J., Reiter, K., Qiao, H., Helm, D., Koch, H., Schoof, M., Canevari, G., Casale, E., Re Depaolini, S., … Kuster, B. (2017). The target landscape of clinical kinase drugs. *Science*, *358*(6367). https://doi.org/10.1126/SCIENCE.AAN4368

Kour, P., Saha, P., Sharma, D. K., & Singh, K. (2024). DNA topoisomerases as a drug target in Leishmaniasis: Structural and mechanistic insights. *International Journal of Biological Macromolecules*, *256*, 128401.

https://doi.org/10.1016/J.IJBIOMAC.2023.128401

Krogh, B. O., & Shuman, S. (2000). Catalytic mechanism of DNA topoisomerase IB. *Molecular Cell*, *5*(6), 1035–1041. https://doi.org/10.1016/S1097-2765(00)80268-3

Kumar Arya, P., Mandal, P., Barik, K., Vijay Singh, D., & Kumar, A. (2024). Computational evaluation of phytochemicals targeting DNA topoisomerase I in Leishmania donovani: molecular docking and molecular dynamics simulation studies. *Journal of Biomolecular Structure and Dynamics*, *42*, 8293–8306. https://doi.org/10.1080/07391102.2023.2256865

Lamba, S., & Roy, A. (2022). DNA topoisomerases in the unicellular protozoan parasites: Unwinding the mystery. *Biochemical Pharmacology*, *203*, 115158. https://doi.org/10.1016/J.BCP.2022.115158

Lee, H., Baek, K. H., Phan, T. N., Park, I. S., Lee, S., Kim, J., & No, J. H. (2021a). Discovery of Leishmania donovani topoisomerase IB selective inhibitors by targeting protein-protein interactions between the large and small subunits. *Biochemical and Biophysical Research Communications*, *569*, 193–198. https://doi.org/10.1016/J.BBRC.2021.07.019

Lee, H., Baek, K. H., Phan, T. N., Park, I. S., Lee, S., Kim, J., & No, J. H. (2021b). Discovery of Leishmania donovani topoisomerase IB selective inhibitors by targeting protein-protein interactions between the large and small subunits. *Biochemical and Biophysical Research Communications*, *569*, 193–198. https://doi.org/10.1016/J.BBRC.2021.07.019

Lobanov, M. Y., Bogatyreva, N. S., & Galzitskaya, O. V. (2008). Radius of gyration as an indicator of protein structure compactness. *Molecular Biology*, *42*(4), 623–628. https://doi.org/10.1134/S0026893308040195

Marquis, J. F., Hardy, I., & Olivier, M. (2005). Topoisomerase I amino acid substitutions, Gly185Arg and Asp325Glu, confer camptothecin resistance in Leishmania donovani. *Antimicrobial Agents and Chemotherapy*, *49*(4), 1441–1446. https://doi.org/10.1128/AAC.49.4.1441-1446.2005

Mathison, B. A., & Bradley, B. T. (2023). Review of the Clinical Presentation, Pathology, Diagnosis, and Treatment of Leishmaniasis. *Laboratory Medicine*, *54*(4), 363–371. https://doi.org/10.1093/LABMED/LMAC134

Michaud-Agrawal, N., Denning, E. J., Woolf, T. B., & Beckstein, O. (2011). MDAnalysis: A toolkit for the analysis of molecular dynamics simulations. *Journal of Computational Chemistry*, *32*(10), 2319–2327. https://doi.org/10.1002/JCC.21787

O'Boyle, N. M., Banck, M., James, C. A., Morley, C., Vandermeersch, T., & Hutchison, G. R. (2011). Open Babel: An Open chemical toolbox. *Journal of Cheminformatics*, *3*(10), 1–14. https://doi.org/10.1186/1758-2946-3-33

Onufriev, A., Bashford, D., & Case, D. A. (2004). Exploring Protein Native States and Large-Scale Conformational Changes with a Modified Generalized Born Model. *Proteins: Structure, Function and Genetics*, *55*(2), 383–394. https://doi.org/10.1002/PROT.20033

Pradhan, S., Schwartz, R. A., Patil, A., Grabbe, S., & Goldust, M. (2022). Treatment options for leishmaniasis. *Clinical and Experimental Dermatology*, *47*(3), 516–521. https://doi.org/10.1111/CED.14919

Redinbo, M. R., Champoux, J. J., & Hol, W. G. J. (2000). Novel insights into catalytic

mechanism from a crystal structure of human topoisomerase I in complex with DNA. *Biochemistry*, *39*(23), 6832–6840. https://doi.org/10.1021/bi992690t

Reguera, R. M., Redondo, C. M., Gutierrez de Prado, R., Pérez-Pertejo, Y., & Balaña-Fouce, R. (2006). DNA topoisomerase I from parasitic protozoa: A potential target for chemotherapy. *Biochimica et Biophysica Acta (BBA) - Gene Structure and Expression*, *1759*(3–4), 117–131. https://doi.org/10.1016/J.BBAEXP.2006.03.006

Saha, S., Acharya, C., Pal, U., Somenath, C., Chowdhury, R., Sarkar, K., Maiti, N. C., Jaisankar, P., & Majumder, H. K. (2016). A Novel Spirooxindole Derivative Inhibits the Growth of Leishmania donovani Parasites both In Vitro and In Vivo by Targeting Type IB Topoisomerase. *Antimicrobial Agents and Chemotherapy*, *60*(10), 6281–6293. https://doi.org/10.1128/AAC.00352-16

Santos-Martins, D., He, Y., Eberhardt, J., Sharma, P., Bruciaferri, N., Holcomb, M., Llanos, M. A., Hansel-Harris, A., Barkdull, A. P., Tillack, A. F., Bianco, G., Paulsen, M. L., Mato, J., Taneja, I., & Forli, S. (2025). Meeko: Molecule Parametrization and Software Interoperability for Docking and Beyond. *Journal of Chemical Information and Modeling*, *65*(24), 13045–13050. https://doi.org/10.1021/acs.jcim.5c02271

Seol, Y., & Neuman, K. C. (2016). The dynamic interplay between DNA topoisomerases and DNA topology. *Biophysical Reviews 2016 8:1*, *8*(1), 101–111. https://doi.org/10.1007/S12551-016-0240-8

Soren, B. C., Dasari, J. B., Ottaviani, A., Iacovelli, F., & Fiorani, P. (2020). Topoisomerase IB: a relaxing enzyme for stressed DNA. *Cancer Drug Resistance*, *3*(1), 18. https://doi.org/10.20517/CDR.2019.106

Souza Silva, J. A., Tunes, L. G., Coimbra, R. S., Ascher, D. B., Pires, D. E. V., & Monte-Neto, R. L. (2021). Unveiling six potent and highly selective antileishmanial agents via the open source compound collection 'Pathogen Box' against antimony-sensitive and -resistant Leishmania braziliensis. *Biomedicine & Pharmacotherapy*, *133*, 111049. https://doi.org/10.1016/J.BIOPHA.2020.111049

Staker, B. L., Hjerrild, K., Feese, M. D., Behnke, C. A., Burgin, A. B., & Stewart, L. (2002). The mechanism of topoisomerase I poisoning by a camptothecin analog. *Proceedings of the National Academy of Sciences of the United States of America*, *99*(24), 15387–15392. https://doi.org/10.1073/PNAS.242259599

Sundar, S., Singh, J., Singh, K., Agrawal, N., Kumar, R., & Singh, V. K. (2024). Current and emerging therapies for the treatment of leishmaniasis Current and emerging therapies for the treatment of leishmaniasis. *Expert Opinion on Orphan Drugs*. https://doi.org/10.1080/21678707.2024.2335248

Takahashi, D. T., Gadelle, D., Agama, K., Kiselev, E., Zhang, H., Yab, E., Petrella, S., Forterre, P., Pommier, Y., & Mayer, C. (2022). Topoisomerase I (TOP1) dynamics: conformational transition from open to closed states. *Nature Communications*, *13*(1), 1–11. https://doi.org/10.1038/S41467-021-27686-7

Valdés-Tresanco, M. S., Valdés-Tresanco, M. E., Valiente, P. A., & Moreno, E. (2021). Gmx_MMPBSA: A New Tool to Perform End-State Free Energy Calculations with GROMACS. *Journal of Chemical Theory and Computation*, *17*(10), 6281–6291. https://doi.org/10.1021/acs.jctc.1c00645

Williams, C. J., Headd, J. J., Moriarty, N. W., Prisant, M. G., Videau, L. L., Deis, L. N., Verma, V., Keedy, D. A., Hintze, B. J., Chen, V. B., Jain, S., Lewis, S. M., Arendall, W. B., Snoeyink, J., Adams, P. D., Lovell, S. C., Richardson, J. S., & Richardson, D. C. (2018). MolProbity: More and better reference data for improved all-atom structure validation. *Protein Science*, *27*(1), 293–315. https://doi.org/10.1002/PRO.3330

Zhang, H., Yan, R., Liu, Y., Yu, M., He, Z., Xiao, J., Li, K., Liu, G., Ning, Q., & Li, Y. (2025). Progress in antileishmanial drugs: Mechanisms, challenges, and prospects. *PLOS Neglected Tropical Diseases*, *19*(1), e0012735. https://doi.org/10.1371/JOURNAL.PNTD.0012735